Supporting Information

Chemical and electrochemical alkali cations intercalation/release in an ionic hydrogen bonded network

Geoffrey Gerer,[a,b] Frédéric Melin,[b] Petra Hellwig,[b] Mir Wais Hosseini[a*] and Sylvie Ferlay[a*]*

[a] Molecular Tectonics Laboratory, University of Strasbourg, UMR UDS-CNRS 7140, Institut le Bel, 4, rue Blaise Pascal, F-67000 Strasbourg, France
ferlay@unistra.fr, hosseini@unistra.fr

[b] Laboratoire de Bioélectrochimie et Spectroscopie, University of Strasbourg, UMR UDS-CNRS 7140, Institut le Bel, 4, rue Blaise Pascal, F-67000 Strasbourg, France
hellwig@unistra.fr

Purity of the used compounds:

Elemental Analysis

Na_2**1**$_3$-$[Fe^{II}(CN)_6]_2$: Elemental analysis calculated (%) for $C_{90}H_{132}Na_2Fe_2N_{24}$ ($Na_2(Fe(CN)_6)_2(C_{26}H_{44}N_4)_3$). MeOH Anal. Calcd.: C 63.3%, H 7.8%, N 19.7%; found: C 63.7%, H 7.6%, N 19.6%.

K_2**1**$_3$-$[Fe^{II}(CN)_6]_2$: Elemental analysis calculated (%) for $C_{90}H_{132}K_2Fe_2N_{24}$ ($K_2(Fe(CN)_6)_2(C_{26}H_{44}N_4)_3$) Anal. Calcd.: C 62.1%, H 7.6%, N 19.3%; found: C 63.4%, H 7.5%, N 19.2%.

Cs_2**1**$_3$-$[Fe^{II}(CN)_6]_2$: Elemental analysis calculated (%) for $C_{90}H_{132}Cs_2Fe_2N_{24}$ ($Cs_2(Fe(CN)_6)_2(C_{26}H_{44}N_4)_3$) Anal. Calcd.: C 56.1%, H 6.9%, N 17.4%; found: C 57.6%, H 6.8%, N 17.3%.

1$_3$-$[Fe^{III}(CN)_6]$: Elemental analysis calculated (%) for $C_{90}H_{132}Fe_2N_{24}$ ($(Fe(CN)_6)_2(C_{26}H_{44}N_4)_3$) Anal. Calcd.: C 65.1%, H 8.0%, N 20.2%; found: C 66.3 7%, H 8.2%, N 20.4%.

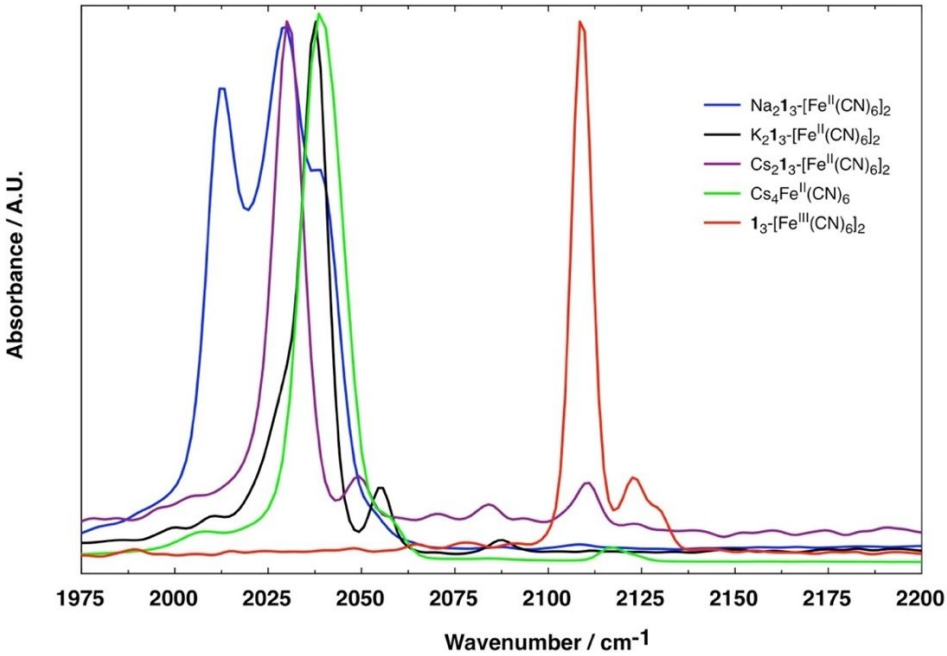

Figure S1: MIR absorbance spectra at room temperature for $X_2\mathbf{1}_3$-$[Fe^{II}(CN)_6]_2$ (X = Na, K and Cs) and $X_2\mathbf{1}_3$-$[Fe^{III}(CN)_6]_2$ together with the one of starting salt $Cs_4[Fe^{II}(CN)_6]$ at RT for the spectral range specific for the $\nu(C{\equiv}N)$ vibrational modes.

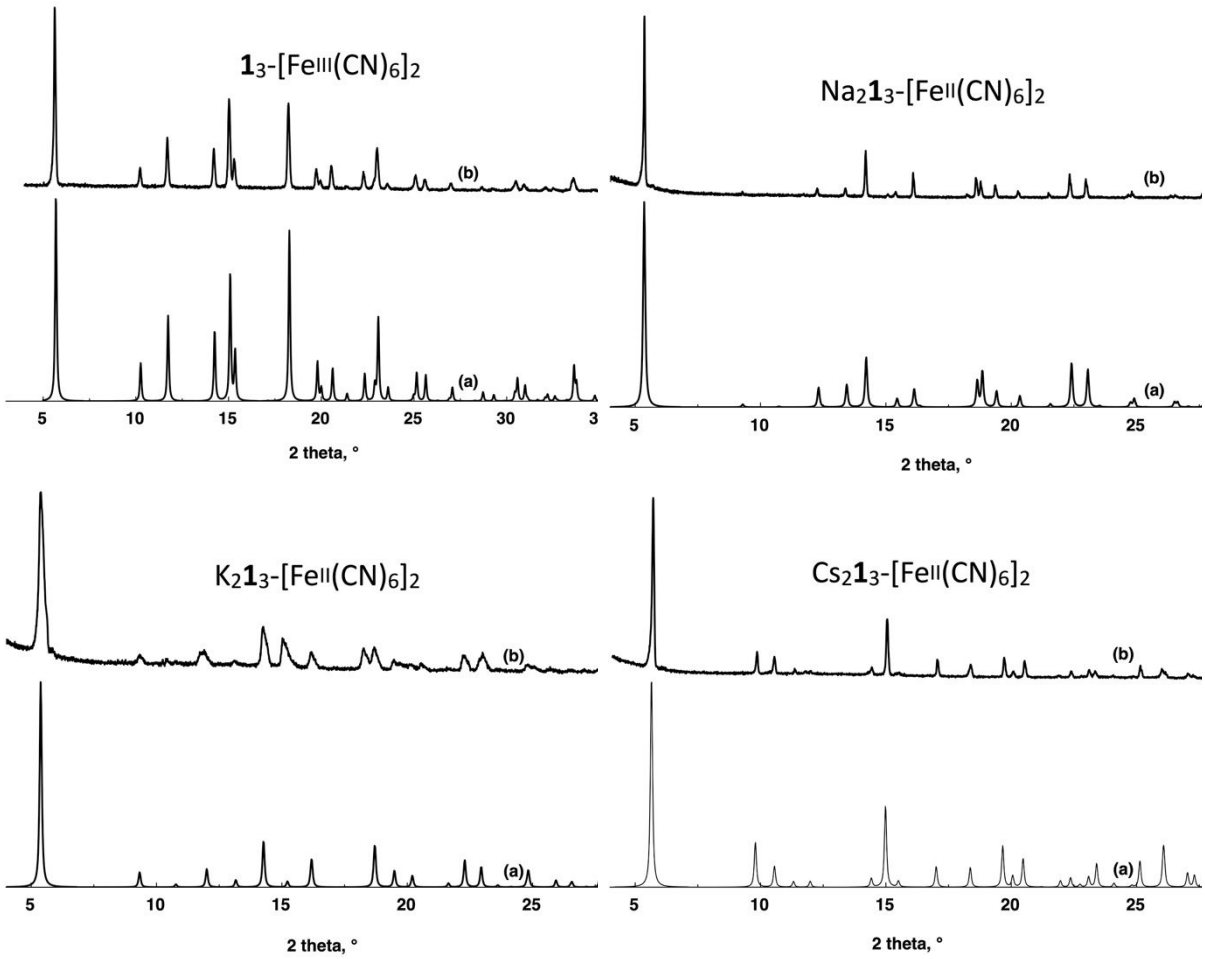

Figure S2: Comparison of the simulated (a) and (b) and recorded PXRD patterns for $\mathbf{1}_3$-$[Fe^{II}(CN)_6]_2$ and $X_2\mathbf{1}_3$-$[Fe^{II}(CN)_6]_2$ (X = Na, K and Cs). Discrepancies in intensity between the observed and simulated patterns are due to preferential orientations of the microcrystalline powders

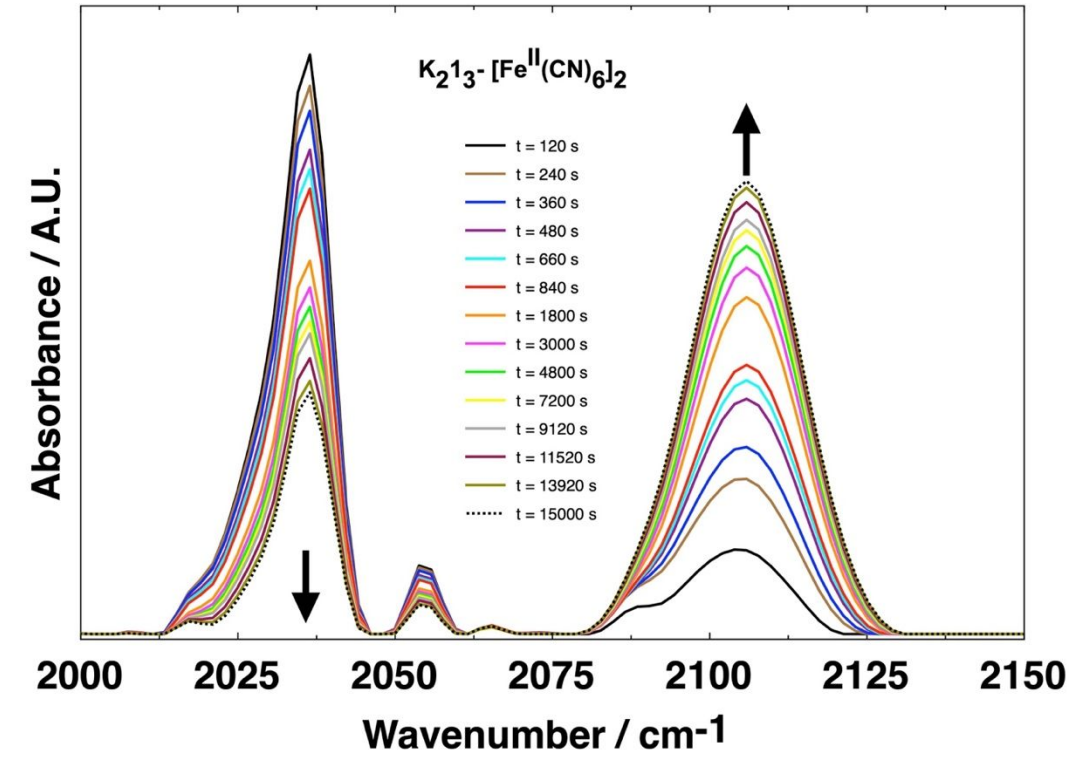

a

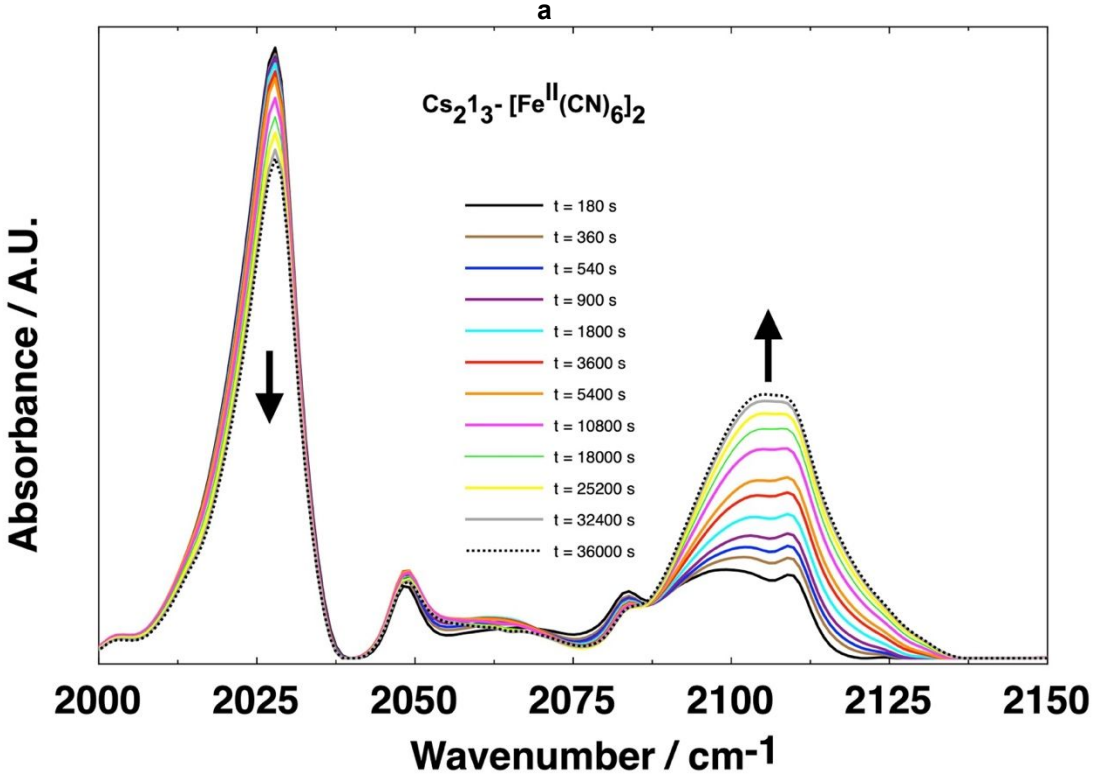

b

Figure S3: Kinetic study of the oxidation of $X_2\mathbf{1}_3$-$[Fe^{II}(CN)_6]_2$ (a) K, b) Cs) into $\mathbf{1}_3$-$[Fe^{III}(CN)_6]_2$ by $S_2O_8^{2-}$ followed at RT by MIR spectroscopy for the 2000-2200 cm^s window.

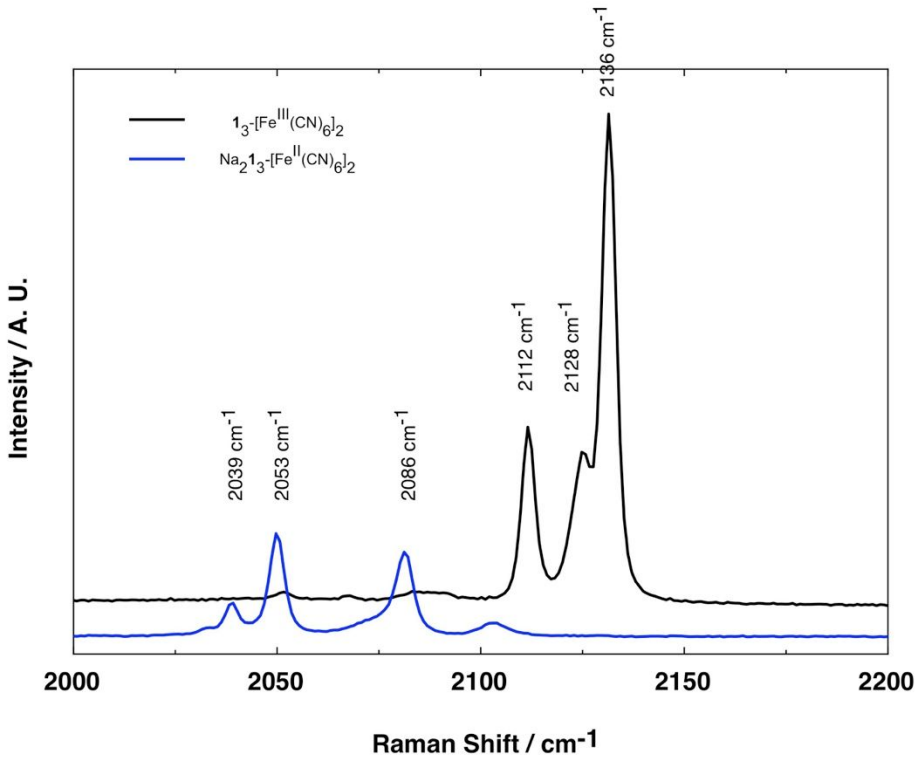

Figure S4: Raman spectra for $Na_2\mathbf{1}_3$-$[Fe^{II}(CN)_6]_2$ and $\mathbf{1}_3$-$[Fe^{III}(CN)_6]_2$ for the 2000-2200 cm^{-1} window.

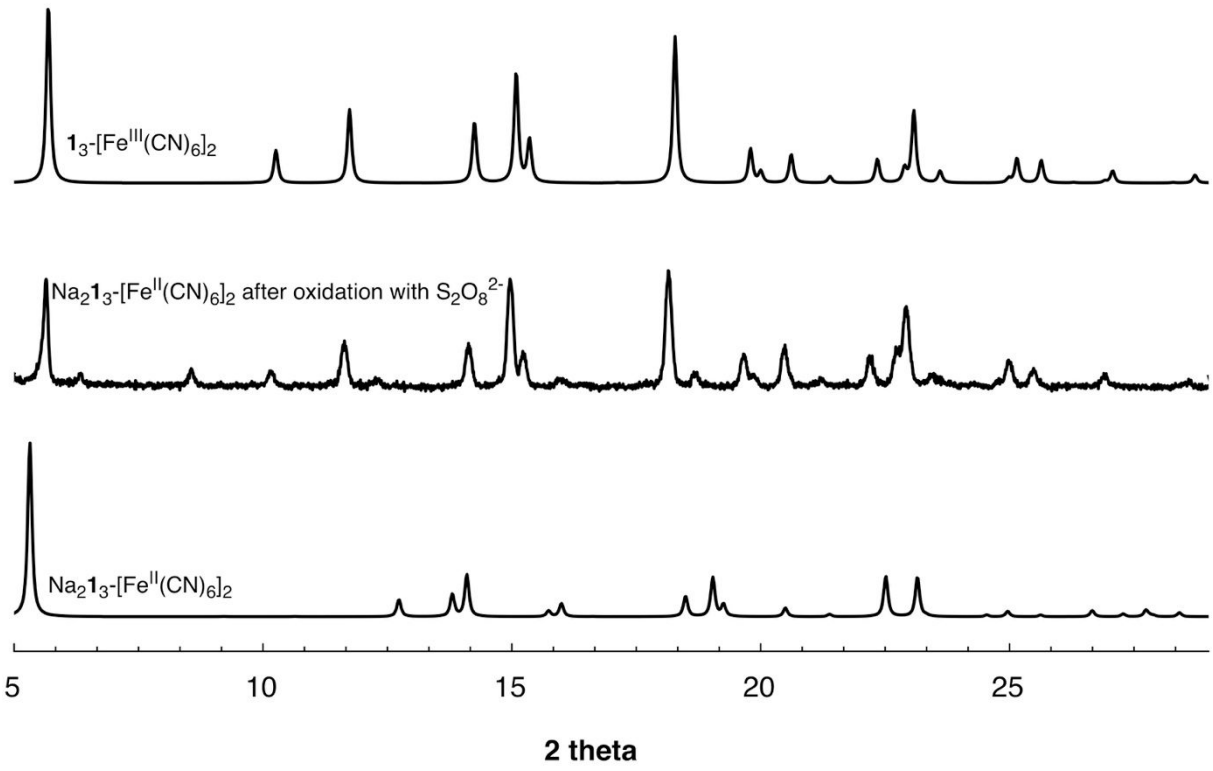

Figure S5: XRPD diagram for $Na_2\mathbf{1}_3$-$[Fe^{II}(CN)_6]_2$ after oxidation by $S_2O_8^{2-}$ and comparison with the simulated XRPD diagrams for $Na_2\mathbf{1}_3$-$[Fe^{II}(CN)_6]_2$ and $\mathbf{1}_3$-$[Fe^{III}(CN)_6]_2$ (from XRD data)

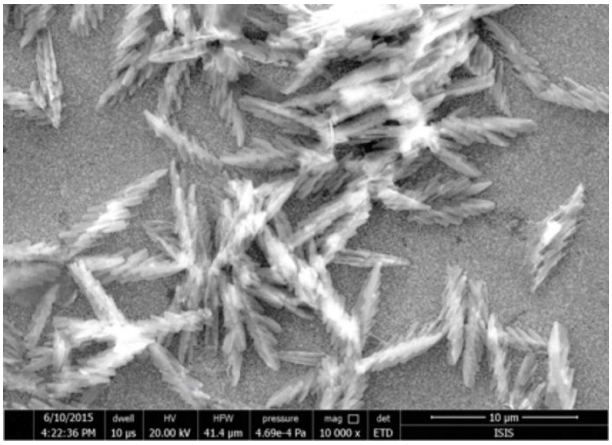

Figure S6: SEM micrograph images of a gold substrate immersed in a solution of **1**-2Cl + $K_3[Fe^{III}(CN)_6]$ in H_2O/MeOH (9/1) after 100 voltammetric cycles between -200 and +800 mV.

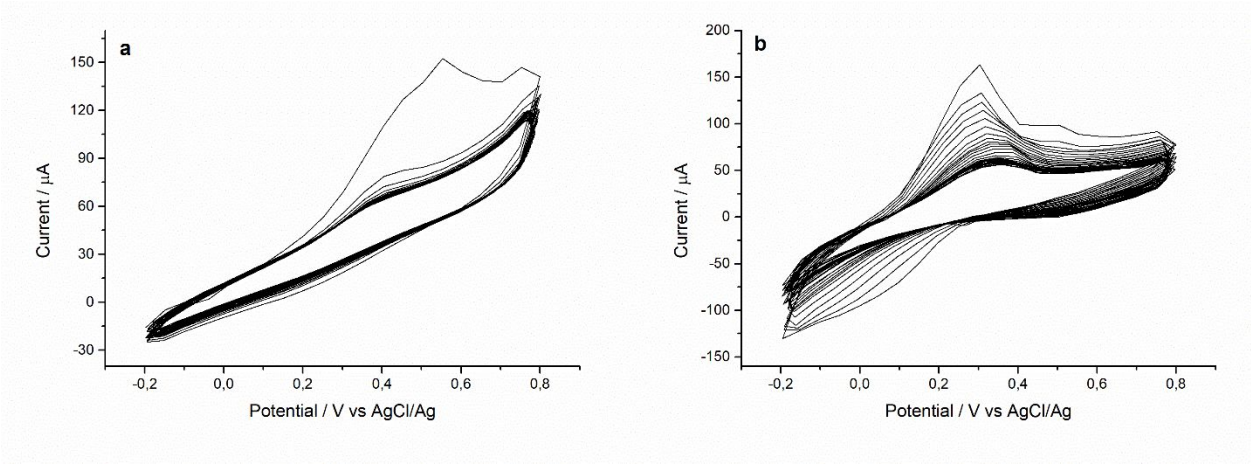

Figure S7: Cyclic voltammograms of gold substrate immersed for 2h into a a solution of (**1**-2Cl + $Na_4[Fe^{II}(CN)_6]$) (a) and (**1**-2Cl + $K_3[Fe^{III}(CN)_6]$) (b). Scan rate 0.1 $V.s^{-1}$.